PROCEEDINGS, 50th Workshop on Geothermal Reservoir Engineering
Stanford University, Stanford, California, February 10-12, 2025
SGP-TR-229

Maximizing the Value of Geothermal Data for Reducing Drilling Risks

Abraham C. Montes, Pradeepkumar Ashok and Eric van Oort

Hildebrand Department of Petroleum and Geosystems Engineering, 200 E Dean Keeton St, Austin, TX 78712, United States

abraham.montes@utexas.edu, pradeepkumar@mail.utexas.edu, vanoort@austin.utexas.edu

Keywords: stuck pipe, risk, drilling data, geothermal, prediction

ABSTRACT

Similar to oil-and-gas wells, drilling risks associated with the occurrence of stuck pipe can be significant also in geothermal well construction, particularly for wells drilled at greater depths in harder rock formations. However, as shown here, such risks can be effectively mitigated by leveraging data acquired from past wells, specifically to evaluate borehole conditions in real time and anticipate potential incidents on new wells. This work presents a multi-agent sticking prediction model, primarily constructed using data from the Utah FORGE geothermal wells, which can be applied for real-time sticking prevention in future wells.

Our proposed model consists of six agents that detect sticking signatures in real time. Each agent operates within a specific variable space designed to clearly differentiate between anomalous data, indicative of stuck pipe signatures, and normal data. These variables combine statistical characteristics, such as the kurtosis and skewness of sensor signals, with physics-based modeling, for example, of drill string friction and cuttings transport. By combining these variables, the agents capture early signs of the primary mechanisms leading to sticking. Ultimately, the agents' predictions are integrated to inform the user, in real time, about the presence, severity, and potential causes of sticking risks. Such information, when presented in a timely fashion, then allows effective mitigation action to be taken

The proposed multi-agent model incorporates four agents related to sticking events that occurred in Utah FORGE wells. These events were primarily attributed to geometric incompatibility between the bottomhole assembly and the borehole, with two instances where insufficient hole cleaning was also a contributing factor. Additionally, the model includes two agents from deep offshore oil-and-gas wells, where similar stuck pipe incidents occurred at greater depths than those in Utah FORGE. We tested this model on the most recently drilled Utah FORGE well, simulating real-time processing of drilling data. Results showed that the model successfully anticipated the sticking event and accurately identified the sticking mechanism. This anticipation was represented by a gradual increase in the sticking risk level within a 35-minute window. This indicates that, if implemented during actual operations, this model could provide the drilling team with timely information about the existence, severity, and causes of sticking risks. This, in turn, enables better-informed decisions and preventative measures, potentially resulting in the avoidance of stuck pipe incidents. While this study focused on stuck pipe prevention, the methodology can be applied to other—equally relevant—drilling risks, such as lost circulation events, wellbore breathing occurrences, well control incidents, etc.

This paper proposes the first multi-agent sticking prediction model that combines statistically derived and model-based variables to provide a timely, comprehensive, and interpretable assessment of sticking risks. We demonstrate that, although geothermal drilling operations are often exposed to significant risks, the proper collection and processing of geothermal data can substantially reduce these risks, ultimately lowering the cost of geothermal well construction.

1. INTRODUCTION

Well construction incidents are events that disrupt drilling operations, requiring immediate, unplanned, and often costly remediation efforts. Examples include severe lost circulation and stuck pipe. The consequences of these incidents depend on their underlying causes and the response of the drilling crew, ranging from hours of non-productive time (NPT) to, in extreme cases, the partial or complete loss of the well.

In geothermal wells, particularly those that target great depths, some drilling risks become amplified, with their likelihood and/or impact (i.e., the cost associated with mitigation/remediation actions) increasing substantially. Some examples of these risks include the following:

- Many geothermal (GT) wells traverse naturally fractured, dry, and under-pressurized formations in overbalanced conditions, making them highly susceptible to severe lost circulation events (van Oort et al. 2021). Notably, some GT anywhere wells such as enhanced geothermal systems (EGS) can benefit from these natural fractures for effective heat extraction. This further amplifies the impact of lost circulation, as plugging or damage to the formation and fractures caused by drilling fluid loss may obstruct the circulation of heat-exchanging fluid through all flow paths in the EGS, ultimately reducing heat extraction efficiency.
- An elevated risk of severe lost circulation is often tied to an increased risk of differential sticking, particularly when drilling through fractured, under-pressurized intervals with substantial overbalance (Shahri et al. 2015). Additionally, in weak, non-cohesive formations, total lost circulation—where no returns are observed at the surface—can lead to wellbore instability. This occurs because a drop in the annular fluid level reduces the radial stress exerted on the borehole wall, sometimes enough to cause wellbore collapse (Winn et al. 2023).

- The construction of high-enthalpy GT wells, especially if performed in zones with an average geothermal gradient [~30°C/km, according to Brommer and O'Sullivan (2020)], generally requires using a small—sometimes slim (with diameters smaller than 5 in.)—drillstring to construct the deepest borehole sections. The mechanical properties of this drillstring generally dictate the maximum tension that can be applied to release it if it becomes stuck. As a result, the risk of stuck pipe at great depths may become significantly higher than at shallow depths due to the reduced likelihood of freeing the string. This, in turn, increases the potential for substantial cost overruns resulting from the additional operations required to continue drilling after an unresolved sticking incident, such as pipe severing, partial borehole abandonment, and sidetracking.

Another factor contributing to the amplification of these risks in deep GT well construction is their impact on the economic feasibility of projects. This is because the levelized cost of energy (LCOE)—the cost per unit of energy, typically measured in kilowatt-hours (kWh), over the entire lifetime of a power-generation project—is generally higher than that of other forms of energy extraction and is highly sensitive to drilling costs (Beckers et al. 2014, Sanyal et al. 2007). High drilling costs resulting from the materialization of drilling risks can lead to GT projects losing competitiveness compared to other energy sources (van Oort et al. 2021).

However, these incidents can be prevented through a three-step process. First, the risk of these incidents occurring must be accurately assessed in a timely manner. Second, the drilling crew must be informed about the risk level and the physical mechanism generating the risk, so that they can select risk-reducing preventive measures when the risk is high. Finally, these measures must be implemented promptly to prevent the risky well condition from escalating into an NPT-producing event. The first two steps of this process are the primary objective of drilling incident prediction models. Therefore, the potential value of these models is in the order of millions of dollars per well [see, for example, Salehi et al. (2022) and Montes et al. (2023)].

Numerous research efforts have focused on constructing such prediction models. Table 1 and Table 2 outline the principal characteristics of previous works on lost circulation and stuck pipe prediction, respectively. In these tables, real-time signals correspond to surface sensor readings, such as hook load and standpipe pressure. Interested readers are encouraged to consult Montes et al. (2024b) for an in-depth review of stuck pipe prediction. Although no dedicated review currently exists for lost circulation prediction models, readers can refer to Feng et al. (2024) and Pang et al. (2022) for an overview of the state of the art. Readers will likely notice similarities between the stuck pipe prediction and lost circulation prediction problems, which, as we argue in this manuscript, can be solved under the same framework.

Table 1: Principal characteristics of recent solutions for lost circulation prediction. A check mark (✓) indicates that the solution uses the referred variable or has the referred limitation. A dash (-) indicates that either the solution does not use the referred variable, does not have the referred limitation, or it is not specified in the referred work. Abbreviations: PPFG=Pore pressure and fracture gradient; Interpret.=Interpretation of the model's prediction; RT=Applicable in real time.

	Considered Variables					Limitations			
Authors	Real-Time Signals	Geological Features	PPFG	Drilling Fluid Properties	Modeling Approach	Precision or Recall <0.8	Lack of Intuitive Interpret.	Not RT	No Risk Level
Ahmed et al. (2020)	✓	-	-	-	Data-driven (radial-basis function network and support vector machine)	-	✓	-	✓
Hou et al. (2020)	✓	✓	✓	✓	Data-driven (feed-forward neural network)	-	✓	-	-
Rotimi et al. (2021)	-	-	-	✓	Data-driven (support-vector machine)	-	✓	✓	✓
Magana-Mora et al. (2021)	✓	-	-	-	Data-driven (random forest and feed-forward neural network)	✓	✓	-	✓
Pang et al. (2022)	✓	-	✓	-	Data-driven (mixture density network)	-	✓	-	-
Wang et al. (2023a)	✓	-	-	✓	Data-driven (long short-term memory network with attention)	-	-	-	✓
Feng et al. (2024)	✓	✓	-	✓	Data-driven (Gaussian mixture, XGBoost and Shapley values)	✓	-	-	✓

Table 2: Principal characteristics of recent solutions for stuck pipe prediction. Symbols and abbreviations used in this table have the same definitions as in Table 1.

	Considered Variables					Limitations			
Authors	Real-Time Signals	Geological Features	PPFG	Drilling Fluid Properties	Modeling Approach	Precision or Recall <0.8	Lack of Intuitive Interpret.	Not RT	No Risk Level
Elahifar and Hosseini (2022)	-	-	-	✓	Data-driven (feed-forward neural network)	✓	✓	✓	✓
Othman et al. (2022)	✓	-	-	-	Data-driven (long short-term memory network)	✓	✓	-	✓
Wang et al. (2023b)	✓	-	-	✓	Data-driven (long short-term memory network)	✓	-	-	-
Montes et al. (2023)	✓	-	-	✓	Data-driven (fuzzy clustering) + physics-based models (torque and drag and cuttings transport)	-	✓	-	-
Kaneko et al. (2024)	✓	-	-	-	Data-driven (non-linear regression) + physics-based insights (torque and drag)	✓	-	-	-
Inoue et al. (2024)	✓	-	-	-	Data-driven (non-linear regression) + physics-based insights (torque and drag)	✓	✓	-	-
Liu et al. (2024)	✓	✓	✓	✓	Data-driven (graph network with attention) + physics-based models (torque and drag and cuttings transport)	-	✓	-	-

While existing solutions have achieved good accuracy in stuck pipe and lost circulation prediction on specific datasets, they still have limitations associated with: (1) linking model predictions to the potential physical mechanisms generating the risk, (2) real-time applicability, which is essential for preventing incidents; (3) spurious predictions of high risk (typically leading to false warnings); and (4) predictions limited to a binary outcome (i.e., whether or not the risk exists), without providing information on the risk level and how it may increase over time. As a result of this limitation, the drilling team may not have enough information to decide on appropriate risk-reduction measures. For example, if a prediction of positive stuck pipe risk is issued, the warning may be insufficient to help the team determine whether stopping for a circulation cycle is necessary or if the risk can be safely managed by simply reducing the tripping speed, without completely stopping the operation.

In this paper, we propose a multi-agent solution for stuck pipe prediction, primarily constructed using data from the Utah FORGE geothermal field, designed to address these limitations. This solution is inherently interpretable, as it links predictions to likely mechanisms of sticking. Additionally, it provides insights into the severity of the sticking condition, from an incipient state to a completely stuck state, enabling the drilling team to design appropriate risk-reduction plans. Finally, it is applicable in real time, facilitating the implementation of measures to prevent costly sticking incidents. While this paper focuses on stuck pipe prediction, which, along with lost circulation, typically accounts for the largest share of NPT in geothermal drilling projects (AlMuhaideb and Noynaert 2021, Purba et al. 2020, Yost et al. 2015), the modeling approach presented here can also be extended to other drilling incidents, such as lost circulation.

The remainder of this paper is organized as follows: First, we introduce the methodology. We then discuss its implementation using the Utah FORGE dataset along with data from wells in the Gulf of Mexico (GoM). Finally, we discuss the results and present the conclusions.

2. METHODOLOGY

The proposed multi-agent solution for stuck pipe prediction consists of four components: (1) the pool of historical agents, (2) the rig state identification agent, (3) the aggregation agent, and (4) the warning generation agent. These components rely on two data sources: real-time signals and contextual data. The first source includes readings from surface rig sensors, such as torque and hook load, while the second consists of variables that remain unchanged for extended periods of time or describe the wellbore configuration, such as the well schematic, well trajectory, and drilling fluid characteristics.

The following paragraphs discuss the objective of each component and how they utilize different data sources to estimate the risk of sticking. Figure 1 illustrates the flow of data from two sources—real-time signals and the contextual data store—to the interface where the sticking risk and associated warnings are displayed. As shown in the figure, the entire process, from data consumption to prediction generation, takes between 1 and 3 seconds using midrange computational resources[1]. The agents involved in this process are described next.

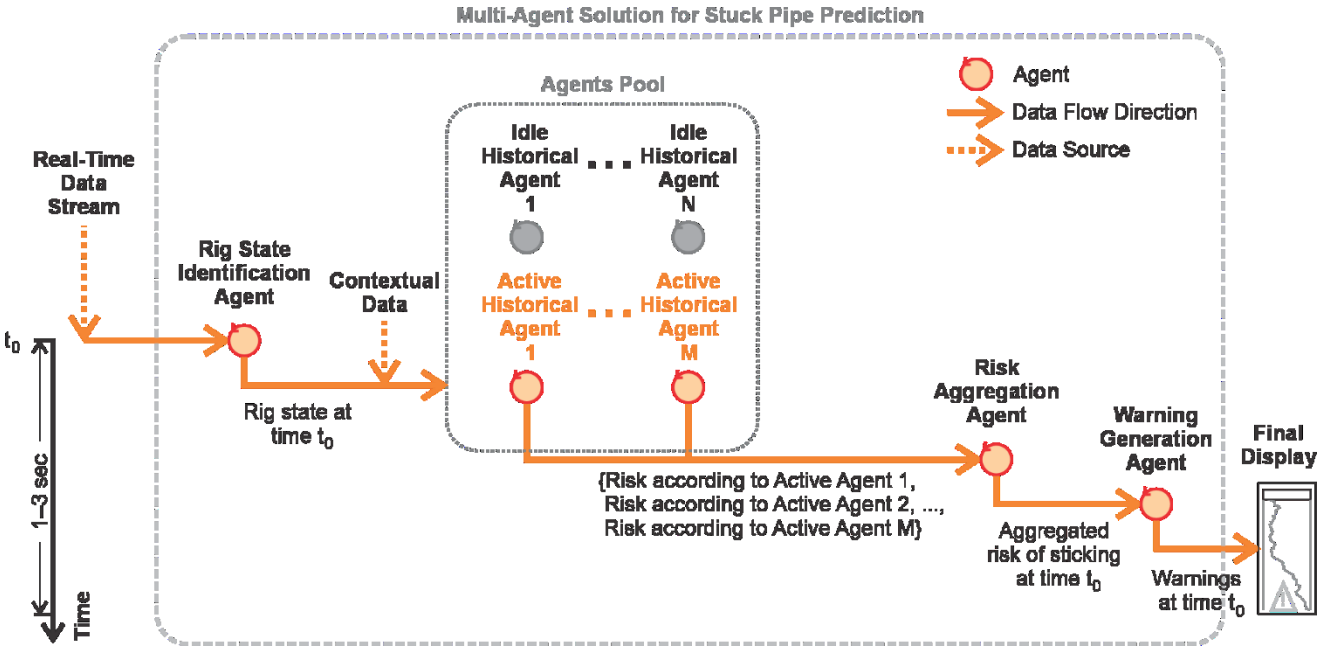

Figure 1: Flow of data from data sources to the final display of sticking predictions. Circles represent the agents in the multi-agent system.

2.1 Pool of Historical Agents

The pool of agents consists of multiple historical agents (denoted as A_i), each with a distinct internal model. Each A_i is associated with a previous stuck pipe event (S_i), that occurred during a specific drilling operation. The complete set of agents is denoted as $\boldsymbol{A}$ (i.e., $\boldsymbol{A} = \{A_1, A_2, \ldots, A_N\}$, where N is the total number of historical agents). The objective of each A_i is to determine whether the current drilling observations resemble past stuck pipe incidents and, if so, to quantify their similarity.

Each agent's model consists of a clustered representation of engineered time-series associated with a past well, where a stuck pipe incident occurred. These time series are not limited to real-time signals. In fact, in the proposed method, none of the agents rely on raw, unprocessed real-time signals. Instead, each agent utilizes functions of real-time signals and contextual data that have been engineered to clearly distinguish between sticking and normal conditions. In other words, in the engineered variable space of A_i, drilling conditions far from S_i form a 'low-risk' cluster, while those near S_i form another cluster, hereafter referred to as the 'high-risk' cluster.

Thus, the objective of each A_i is to identify signatures of past stuck pipe incidents in the current well and assess their significance. Each agent first transforms the current drilling conditions into its unique engineered variable space, where predefined risk-related clusters exist. The agent then evaluates the proximity of the drilling conditions to the low- and high-risk clusters as a proxy for the sticking risk level.

Here, we have provided a high-level overview of historical agents. The discussion on agent construction is postponed until Section 2.5 to first provide a general system overview.

[1] A computer whose performance falls between a microcomputer and a mainframe. e.g., a computer with an Intel Core i7 2.5-GHz CPU, an NVIDIA RTX 3050 GPU, and 8–16 GB of RAM.

2.2 Rig State Identification Agent

The rig state identification agent categorizes the drilling activity at each moment into one of eleven classes: drilling in rotary mode, drilling in slide mode, reaming, backreaming, washing down (tripping in with pumps), pumping out (tripping out with pumps), tripping in on elevators, tripping out on elevators, circulating, string set in the slips, and string off the slips. These categories are mutually exclusive, meaning the rig cannot perform more than one at the same time.

This agent plays a crucial role in estimating stuck pipe risk. Although multiple agents exist in $\boldsymbol{A}$, only those relevant to the current rig state contribute to risk estimation. Specifically, agents A_i associated with stuck pipe events that occurred under different rig states remain idle, while those matching the current rig state evaluate the drilling conditions and generate a risk prediction. The aggregation agent then consolidates these individual assessments into a single risk evaluation, which we describe next. We denote the set of idle agents as $\boldsymbol{P'}$ and the set of active agents as $\boldsymbol{P}$, such that $\boldsymbol{P} \cup \boldsymbol{P'} = \boldsymbol{A}$.

The rig state identification agent processes real-time signals, buffers 30 seconds of data, and determines the rig state using a transformer-based classifier. This classifier consists of six transformer layers, each with 256-dimensional embeddings and eight attention heads. For further details on the transformer-based classifier, see Montes et al. (2025).

2.3 Aggregation Agent

The aggregation agent consolidates predictions from the selected, active agents in $\boldsymbol{P}$. To achieve this, the agent leverages contextual data from each A_i. Specifically, it considers the hole size at which the sticking incident associated with A_i occurred, the type and flexural rigidity of the bottomhole assembly (BHA) that became stuck, the borehole inclination at the sticking point, the drilling fluid type, and the rock strength at the sticking interval. These characteristics are compiled into a vector for each A_i, denoted as $\overrightarrow{C_i}$.

Similarly, the same information for the current well—where the model predicts the sticking risk—is compiled into a context vector, denoted as $\overrightarrow{C_w}$. The aggregation agent weights each active agent's contribution to the final sticking risk estimate based on the Euclidean distance between context vectors:

$$R = \frac{1}{\sum_{j:A_j \in \boldsymbol{P}} w_j} \sum_{j:A_j \in \boldsymbol{P}} R_j \, w_j \tag{1}$$

Here, R is the aggregated sticking risk level, R_j represents the risk estimate made by the j-th historical agent, and w_j is the weight of the j-th historical agent, which in turn, can be calculated as follows:

$$w_j = 1 - \exp\left[\frac{-\left(\left\|\overrightarrow{C_J} - \overrightarrow{C_w}\right\|_2\right)^2}{2\sigma^2}\right] \tag{2}$$

Here, σ is a trainable parameter that determines the loss of influence in the aggregate risk estimate with well dissimilarity. In other words, it determines how irrelevant are the agents whose associated well is highly dissimilar to the well under analysis. It is worth noting that the function defining w_j is a radial basis function.

2.4 Warning Generation Agent

The objective of this agent is to issue warnings (which are a binary output) when the aggregated risk estimate exceeds a threshold. Such a threshold is a trainable parameter that determines the level of risk tolerance. It is worth noting that while this agent generates a binary output, the aggregation agent produces a continuous, normalized output that can be interpreted as a measurement of the sticking risk level.

2.5 Construction of Historical Agents

Historical agents are constructed in three steps. First, each historical stuck pipe incident is analyzed to identify (1) the sticking mechanism (e.g., whether it occurred due to uncontrolled solids accumulation, geometric incompatibility between the BHA and the borehole, or excessive overbalance); (2) observable early signs in real-time signals (e.g., erratic torque fluctuations before the BHA became stuck); and (3) engineered variables that could have aided early detection of sticking (e.g., the proximity of a highly rigid BHA section to a high-curvature interval or an interval with accumulated, non-evacuated cuttings). Both real-time signals and engineered variables are time series, recorded/computed typically at a frequency of 1 Hz (Thonhauser et al. 2007).

In the second step, these engineered variables—derived from the identified sticking mechanism—are evaluated for their effectiveness in distinguishing normal from sticking conditions. Effective variables should exhibit distinct behavior as the incident approaches, compared to periods when the BHA was free under the same rig state. This distinction is assessed using the Kolmogorov-Smirnov hypothesis test across multiple time windows. The test evaluates whether drilling conditions near the stuck pipe event originate from a statistically different distribution than those observed earlier. A significant shift is interpreted by our model as an increase in sticking risk.

Variables passing the test (i.e., with a p-value greater than 0.05) are then used for clustering. Clusters are generated using the fuzzy c-means algorithm (Bezdek et al. 1984), which iteratively estimates the centroids (i.e., the mean of grouped observations) for a predefined number of clusters. By incorporating fuzzy logic, cluster boundaries remain 'flexible' rather than sharply defined. Thus, the transition

from low to high sticking risk is gradual rather than abrupt. The degree of this transition is controlled by a tunable parameter—the fuzziness coefficient.

Equation 3 is minimized iteratively to estimate the centroids of the clusters in each iteration and the membership matrix, respectively.

$$J(\boldsymbol{C}) = \sum_{k:\boldsymbol{c}_k \in \boldsymbol{C}} \sum_{i:\boldsymbol{x}_i \in \boldsymbol{X}} \mu_{i,k}^{\eta} \|\boldsymbol{x}_i - \boldsymbol{c}_k\|_2 \tag{3}$$

Here, $\boldsymbol{X}$ is the set of all observations, $\boldsymbol{x}_i$ represents the i-th observation of the drilling condition—whose dimensionality corresponds to the number of selected variables—, $\mu_{i,k}$ is the membership value of the drilling condition $\boldsymbol{x}_i$ to the k-th risk-related cluster, and $\boldsymbol{C}$ is the set of all clusters' centroids.

Importantly, the membership values, $\mu_{i,k}$, quantify the extent to which the drilling conditions belong to each cluster at any given time. In other words, these values encode the sticking risk level, indicating how advanced the sticking condition is—from an incipient state to an impending fully stuck situation.

It is worth noting that the number of clusters, $|\boldsymbol{C}|$, is predefined before iteratively solving for their centroids and the observations' membership values. While one could impose two clusters based on a binary risk classification (low and high), we determine the optimal number of clusters using the fuzzy partition coefficient (FPC). This coefficient, ranging from 0 to 1, measures how well the clusters represent the data. Specifically, each agent's model is constructed multiple times with different cluster numbers, and the FPC is computed for each configuration. The final model—and its corresponding number of clusters—is selected based on the highest FPC value.

In this section, we have outlined the functionality of each component of the sticking-prediction system and the construction of historical agents. In the next section, we will present the system's implementation using the Utah FORGE geothermal wells and describe the engineered variable spaces associated with these agents.

3. RESULTS

This section is divided into two parts. First, we describe the sticking incidents that were used to construct the current set of historical agents in our multi-agent system. Subsequently, we showcase the testing of the multi-agent solution with data from the Utah FORGE well 16B(78)-32—the production well.

3.1 Stuck Pipe Incidents Analyzed for Model Construction

Currently, five wells with a total depth (TD) greater than 7,500 ft have been drilled in the Utah FORGE geothermal field. These include an injector well and a production well, named 16A(78)-32 and 16B(78)-32, respectively, which, together with the igneous rocks and fracture network in the subsurface, form an EGS. Additionally, there are three observation/seismic-monitoring wells, named 78B-32, 56-32, and 58-32.

Figure 2 shows the as-drilled well schematics along with the points where sticking incidents occurred along the boreholes. As depicted, three of these incidents took place during tripping, while the remaining two occurred while drilling (with the bit on bottom). In the following paragraphs, we provide a concise yet comprehensive summary of these incidents and their potential causes. Interested readers may refer to Montes et al. (2023) and Montes et al. (2024a) for a more detailed analysis supporting these summaries.

3.1.1 Stuck Pipe Incident in Well 16A(78)-32

The stuck pipe incident occurred at a measured depth (MD) of 6,507 ft in the 8-3/4 in. borehole section. The incident took place while drilling in slide mode through granite with a water-based mud (WBM) of 8.9 ppg density. The bottomhole assembly (BHA) included a polycrystalline diamond compact (PDC) bit, a mud motor with a 1.5° bend, and a string stabilizer with an outer diameter (OD) of 8-5/8 in. The drillstring became stuck after the borehole reached an inclination of 20°.

An in-depth analysis, including hole cleaning simulations and an assessment of potential borehole instability, concluded that the incident was purely geometric in nature. It was primarily caused by the string stabilizer placed on top of the mud motor becoming stuck in an interval with a sudden and pronounced variation in borehole diameter, potentially also associated with a high, localized curvature (Montes et al. 2023).

3.1.2 Stuck Pipe Incident in Well 56-32

The sticking incident occurred at 5,790 ft MD in the 8-3/4 in. borehole section while tripping in the hole on elevators with BHA No. 12—a highly rigid BHA consisting of a mud hammer and two full-gauge string roller reamers. Notably, while performing releasing maneuvers (applying tension), the driller maintained full circulation with no indications of annular obstructions.

A comprehensive analysis of the event concluded that the sticking incident was purely geometric (Montes et al. 2023). It occurred when the most rigid part of the BHA passed through an interval with high localized curvature, where the verticality of the borehole trajectory was temporarily lost. This hypothesis was supported not only by observations during incident management but also by subsequent operations. More flexible BHAs run later showed significantly improved tripping efficiency after reaming through the problematic interval, likely correcting the localized high curvature.

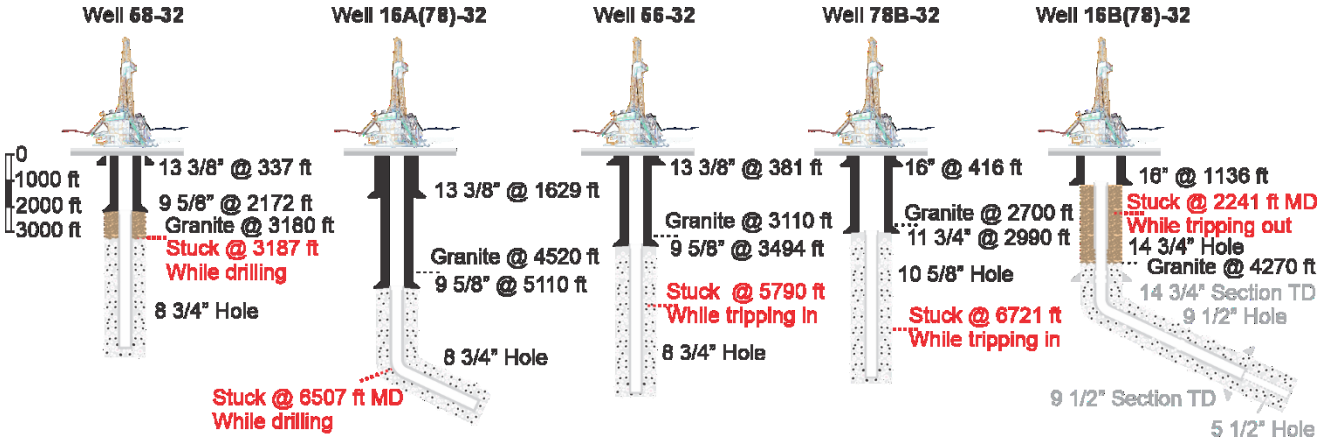

Figure 2: As-drilled well schematics of Utah FORGE wells with a TD deeper than 7,500 ft. The depths where the drillstring became stuck are highlighted in red [adapted from Montes et al. (2024a)].

3.1.3 Stuck Pipe Incident in Well 78B-32

Similar to the previously described incident, this event occurred while tripping in on elevators, but in the 10-5/8 in. hole section while running a directional BHA. The BHA consisted of a mud motor with a 1.15° bent and two string stabilizers with blade ODs of 10-1/4 in. and 10-1/2 in., respectively. Unlike the incident in well 56-32, full circulation with normal pumping pressure was not immediately possible after the incident. Circulation was only restored after rotating the string.

A detailed analysis of this event, which included borehole stability and hole cleaning assessments, determined that the incident was primarily related to geometry, with a potential contribution from accumulated solids at the bottom of the hole (Montes et al. 2023). The analysis revealed that the BHA that became stuck had significantly different rigidity compared to the preceding BHA, which was used for correcting the under-gauge hole (1-7/8 in. under the bit size due to coring operations). This difference in rigidity likely contributed to a high localized curvature, evidenced by an increase in variability in the hook load signal while tripping in the hole.

Additionally, it was found that the time spent circulating with the previous BHA, using a low-carrying-capacity WBM, was insufficient to evacuate the generated cuttings. The volume of cuttings required to fill the deepest 21-ft interval of the hole, where the BHA became stuck, closely matched the volume of cuttings generated with the previous BHA. The contribution of these solids to the sticking incident explains the circulation restriction observed while attempting to release the string.

3.1.4 Stuck Pipe Incident in Well 58-32

The incident occurred in the 8-3/4 in. hole section at 3,187 ft MD, while drilling in rotary mode through the transition from alluvium to granite. The stuck BHA consisted of a tricone bit, a mud motor, and two string stabilizers. The string was released through jarring maneuvers, which resulted in a motor sleeve blade being left in the hole.

A thorough analysis of the event revealed that the incident was likely geometric, with the BHA becoming stuck at the transition from alluvium to granite (Montes et al. 2023). Evidence supporting this hypothesis included (1) the torque spikes observed before the BHA's integrity failure (the motor's sleeve losing a blade) while entering the granite transition, and (2) the sharp, notable change in borehole diameter—evident in the caliper log—at the transition point, where the BHA became stuck.

3.1.5 Stuck Pipe Incident in Well 16B(78)-32

The incident occurred while tripping out of hole on elevators through the alluvium formation at 2,241 ft MD in the 14-3/4 in. borehole section. The BHA consisted of a PDC bit, a mud motor, and a string stabilizer. The hole was drilled with a WBM of 9 ppg density. The incident was characterized by highly restricted string movement upwards, accompanied by several pressure spikes. Although the completely stuck condition lasted no longer than 0.5 hours, a partial sticking condition persisted, slowing down tripping progress.

A comprehensive analysis of the event revealed that the incident was primarily related to insufficient hole cleaning, with potential geometric contributing factors (Montes et al. 2024a). It was found that a significant concentration of cuttings remained in the hole when circulation was stopped, which may have been dragged along with the BHA to the point where it became stuck. Furthermore, the string became stuck at the transition from fine sand to markedly coarse sand. While it is unlikely that this transition caused a sudden change in borehole diameter, we hypothesize that it may have contributed to wedging the dragged cuttings, ultimately leading to the sticking incident.

In addition to the Utah FORGE wells, our multi-agent system also incorporates two agents associated with deep offshore wells in the Gulf of Mexico (GoM), anonymized as Well A and Well B. The stuck pipe incidents in these wells are described below:

3.1.6 Stuck Pipe Incident in Well A

The sticking incident in this well occurred in the 9-7/8 in. borehole section, which began at 18,651 ft MD with 22° of inclination and reached its TD at 29,495 ft MD with 23° of inclination. The section was drilled using synthetic-based mud (SBM) and was partially underreamed (opened to 10-5/8 in.) from the previous casing shoe to 26,791 ft—approximately 200 ft MD below the base of a salt structure. The stuck pipe incident involved BHA No. 5, which had drilled the entire borehole section. The BHA consisted of a PDC bit, a push-the-bit rotary steerable system (RSS), a set of logging-while-drilling (LWD) tools, including tools for resistivity, gamma ray, multipole sonic, and annular pressure measurements; a total of 6 string stabilizers with a blade OD of 9-3/4 in.; an underreamer; 6-3/4 in. drill collars; 5-7/8 in. heavy-weight drill pipe (HWDP); and a combined drill pipe string consisting of 5-7/8 in. and 6-5/8 in. pipes.

The sticking incident occurred while tripping after reaching the TD of the borehole section. The crew circulated to condition the drilling fluid, increasing its density from 14.9 ppg to 15.2 ppg, and to evacuate the generated cuttings from the well. While tripping out of hole, the drilling crew noticed abnormal pressure behavior, erratic torque when backreaming, and excessive drag. They decided to trip back in to the bottom to ensure good borehole condition prior to running the casing string. However, after running the BHA in on elevators and attempting to establish circulation just 100 ft above the bottom, pressure spiked and the drillstring became stuck. The crew managed to pull the string out by working with tension for six hours and eventually re-established circulation. Real-time signals associated with this incident are shown in Appendix A, Figure A1.

A deeper analysis of the event revealed that it was likely associated with two mechanisms. First, the gamma-ray log indicated significant lithological variation in this section. A caliper log from an offset well in the same borehole section revealed that these variations contributed to high fluctuations in borehole diameter. These diameter variations, in particular sudden diameter reductions, can act as wedges, allowing even small volumes of cuttings to accumulate and cause sticking. Second, despite the low inclination of the borehole (23°), cuttings accumulation—both from drilling and backreaming—could occur in two forms: as a refill at the bottom and as isolated accumulations at sudden changes in borehole diameter.

3.1.7 Stuck Pipe Incident in Well B

The incident in Well B occurred in the 5-7/8 in. borehole section, which started at 27,570 ft MD with 30° of inclination and reached its TD at 28,106 ft MD with 34° of inclination. The section was drilled using a fluid suited for reservoir drilling (drill-in fluid), with a multistabilizer BHA (lacking sophisticated deviation-control tools). This BHA consisted of a PDC bit, three stabilizers with a blade OD of 5-5/8 in., and an underreamer to open the hole to 7 in. The BHA was successfully retrieved to the surface after reaching TD.

Following this, a set of open-hole logs was run in the hole using e-line. Immediately afterward, the drilling team ran BHA No. 8, intended to condition the hole after logging and to displace to clean fluid. However, this BHA became stuck while approaching the bottom of the hole. After intense jarring operations, the BHA parted. The crew pulled the remainder of the BHA to the surface, leaving a fish in the borehole, necessitating a sidetrack in a well that had already landed in the target and reached TD. Appendix A, Figure A2 shows the real-time signals recorded before and after the incident. As indicated in the figure, the event was characterized by the inability to establish circulation or rotation.

A thorough analysis of the event suggests that accumulated solids in the borehole were likely the cause of the incident when the bit was run on elevators through them. This hypothesis is supported by three key observations. First, a transient cuttings transport simulation of the drilling, circulation, and tripping operations indicated that a fraction of the generated cuttings was not effectively evacuated, potentially accumulating at the bottom of the hole. Second, the back-calculated friction factor while approaching the bottom of the hole exhibited high variability—an indication often associated with cuttings accumulation on the low side of the borehole (see Appendix A, Figure A3). Finally, the inability to circulate (see Figure A2) suggests that material, likely cuttings, blocked the annular space between the drillstring and the borehole wall.

It is also important to note that the drilled reservoir has a long production history, resulting in a notable decline in pore pressure. This led to the hypothesis that the drillstring may have become differentially stuck, rather than packed off by solids. However, this hypothesis does not explain the inability to circulate, nor does it account for the sudden nature of the incident. The incident occurred without any indications of potential sticking during connections—when the drillstring remains static while set in the slips—and with no apparent time dependency, a characteristic feature of differential sticking (Dupriest et al. 2011).

3.2 Variables for Stuck Pipe Prediction

Based on the analyses summarized in the previous paragraphs, we generated an initial set of variables that could potentially differentiate normal conditions from risky, sticking conditions for each event. These variables were derived as new, engineered time series variables from the original real-time signals and contextual data. We then assessed the significance of these variables by conducting the statistical tests described in Section 2.5.

To ensure that the derived variables are indexed in time (i.e., that they form time series), enabling real-time prediction of sticking risk, we applied a sliding time window over the real-time signals and incorporated contextual data where necessary. The width of this sliding window is not uniform across all features. Instead, it is fine-tuned for each variable to maximize the distinction between sticking and normal conditions. We represent this window as $\boldsymbol{W}$, a set of S time-indexed observations ($\{w_1, w_2, w_3, \dots, w_S\}$).

In the following paragraphs, we describe some of the selected variables and their respective definitions. Variables not included in this discussion follow a similar approach. For instance, the window-based variance of the torque signal is implemented in the same way as the

window-based variance of the hook load. Interested readers are encouraged to consult Montes et al. (2023) and Montes et al. (2024a) for additional details on both the variables described here and those omitted for brevity.

3.2.1 Variability of the Back-Calculated Friction Factor

This variable captures the variance of the friction factor. Increasing resistance to pipe movement is expected to cause high variance in this friction factor. The friction factor is estimated, at each point in time, by solving the following equation:

$$\min_{\mu(t)}\{H(t) - [B + F(\mu, s)|_{s=0}]\} \tag{4}$$

Here, $\mu(t)$ is the friction factor at time t, s is the MD, $H(t)$ is the hook load reading at time t, B is the block weight, and $F(\mu, s)|_{s=0}$ is the estimated tension at the surface, which is the solution to the following ordinary differential equation, evaluated at the surface ($s = 0$):

$$\frac{dF}{ds} + w_b \cos\alpha \pm \mu \sqrt{\left(F\,\frac{d\alpha}{ds} - w_{bp}\sin\alpha\right)^2 + \left(F\sin\alpha\,\frac{d\theta}{ds}\right)^2} = 0 \tag{5}$$

Here, w_b is the string weight, corrected for buoyancy, α is the hole inclination, and θ is the hole azimuth. This equation corresponds to the well-known soft-string drag model (Johancsik et al. 1984), which neglects the bending stiffness of the drillstring and assumes that the drillstring follows the same trajectory as the borehole.

Intuitively, the resulting friction factor is the one that produces the closest estimate of the observed hook load at each point in time. Solving Equations 4 and 5 results in a time series of friction factors. The variance of the friction factor is then calculated as follows:

$$\sigma_\mu^2(t) = \frac{1}{|\boldsymbol{W}| - 1} \sum_{\mu_i \epsilon \boldsymbol{W}(t)} [\mu_i - \bar{\mu}(t)]^2 \tag{6}$$

Here, $\sigma_\mu^2(t)$ is the variance of the friction factors that fall within the time window $\boldsymbol{W}$. This variance changes at each time t because $\boldsymbol{W}$ is a sliding window. μ_i represents the i-th friction factor within $\boldsymbol{W}$ at time t, and $\bar{\mu}(t)$ is the mean of friction factors within $\boldsymbol{W}$.

3.2.2 Rate of Change of the Back-Calculated Friction Factor

This variable captures the rate and direction of change of the back-calculated friction factor. Geometric sticking is expected to show higher rates of change compared to other types of sticking, as the increase in resistance to movement typically occurs within a shorter timeframe (depending heavily on the tripping speed). In contrast, non-sticking, normal conditions are expected to show little to no rate of change in the friction factor. Similar to the previous variable, this one relies on the solutions to Equations 4 and 5. The rate of change is calculated using a 3-point backward difference, as follows:

$$\dot{\mu}(t) = \frac{3\mu(t) - 4\mu(t-1) + \mu(t-2)}{2\,\Delta t} \tag{7}$$

Here, $\mu(t)$ is the back-calculated friction factor at time t, $\dot{\mu}(t)$ is its rate of change, and Δt is the time between subsequent observations of the drilling process (typically, 1 s).

3.2.3 Kurtosis of the Hook Load Signal

This variable characterizes the heaviness of the tails in the hook load distribution within the sliding window $\boldsymbol{W}$. In cases of moderate restriction to pipe movement, the tails are expected to be narrower, resulting in a higher peak of the distribution. The intuition behind this variable is illustrated in Figure 3 and discussed in more detail later in this section. The variable is calculated as follows:

$$K(t) = \left\{\frac{1}{|\boldsymbol{W}|}\sum_{H_i \epsilon \boldsymbol{W}(t)} [H_i - \bar{H}(t)]^4\right\}\left\{\frac{1}{|\boldsymbol{W}|}\sum_{H_i \epsilon \boldsymbol{W}(t)} [H_i - \bar{H}(t)]^2\right\}^{-2} \tag{8}$$

Here, $K(t)$ is the hook load kurtosis at time t, H_i is the i-th hook load value that falls within $\boldsymbol{W}$, and $\bar{H}(t)$ is the mean hook load in $\boldsymbol{W}$.

3.2.4 Mean of the BHA Flexural Rigidity Difference with its Predecessors

This variable serves as a proxy for the difference in stiffness between the current BHA and the previous BHAs used to drill the intervals encountered while tripping. The stiffness of the BHA, in conjunction with other factors such as bit-rock interaction, determines the amount of deflection the BHA experiences while drilling the borehole. This deflection influences the borehole curvature and the potential formation of undulations—particularly when the drillstring becomes directionally unstable (Marck and Detournay 2016, Pastusek and Brackin 2003). In essence, the BHA's stiffness may leave a 'fingerprint' on the drilled borehole geometry. If a BHA with significantly different rigidity is run in the borehole, it is likely to encounter movement restrictions, as observed in wells 56-32 and 78B-32, and discussed in stuck pipe prevention guidelines, such as Mitchell (2014) and Bowes and Procter (1997). The difference in BHA flexural rigidity can be estimated as follows:

$$\Delta R(t) = \frac{1}{L_{BHA}} \int_{z_{Bit}(t)-L_{BHA}}^{z_{Bit}(t)} [R_{BHA}(z) - R_{Hole}(z)]dz \tag{9}$$

Here, $\Delta R(t)$ is the mean flexural rigidity difference between the current BHA and the 'fingerprinted' rigidity in the hole, L_{BHA} is the BHA length, $z_{Bit}(t)$ is the bit depth at time t, $R_{BHA}(z)$ is the BHA rigidity at depth z and $R_{Hole}(z)$ is the average rigidity of the BHA used to drill the interval at depth z. The rigidity $R_{BHA}(z)$, in turn, can be estimated as follows:

$$R_{BHA}(z) = E(z) \frac{\{[D_o(z)]^4 - [D_i(z)]^4\}}{64} \tag{10}$$

Where $E(z)$ is the Young's modulus of the BHA component located at depth z; and $D_o(z)$ and $D_i(z)$ are its external and internal diameters, respectively.

It is worth noting that while $\Delta R(t)$ is expressed as an integral, it can be approximated as a summation. In practice, $R_{BHA}(z)$ typically remains constant along a single BHA component—assuming all components are cylindrical, with no significant cross-sectional area variations. Similarly, $R_{Hole}(z)$ remains the same for the entire footage of (i.e., the interval drilled with) a previous BHA. It is worth noting that $R_{BHA}(z)$ is simply the product of the component's Young's modulus and its moment of inertia. Lastly, it is important to highlight that Equation 9 results in a time series output, as the bit position changes over time, which in turn alters the limits of the integral.

3.2.5 BHA Curvature Exposure

This variable captures whether the contact points, at each point in time, traverse intervals with high curvature, where the BHA may become geometrically stuck—similar to the incident in well 56-32. This variable is engineered to increase when a rigid portion of the BHA moves through high-tortuosity intervals. We estimate this variable as follows:

$$\kappa(t) = \frac{1}{L_{BHA}} \int_{z_{Bit}(t)-L_{BHA}}^{z_{Bit}(t)} [\dot{\tau}(z) \cdot R_{BHA}(z)]dz \tag{11}$$

Here, $\kappa(t)$ is the mean BHA curvature exposure at time t, and $\dot{\tau}(z)$ is the rate of change, in depth, of the tortuosity index at depth z. The tortuosity index, $\tau(z)$, is calculated as follows:

$$\tau(z) = \sqrt{\tau_i(z)^2 + \tau_a(z)^2} \tag{12}$$

Here, $\tau_i(z)$ and $\tau_i(z)$ are the inclination and azimuth components of the tortuosity index, respectively. These components can be calculated as follows:

$$\tau_i(z) = \frac{20 \times 10^3 \cdot f_{SF}\, |\boldsymbol{N_i}|}{L_c} \sum_{j:n_j \in \boldsymbol{N_i}} \left[\left(\frac{L_{cj}}{L_{xj}} - 1\right) \cdot w_i\right] \cdot f \tag{13}$$

$$\tau_a(z) = \frac{20 \times 10^3 \cdot f_{SF}\, |\boldsymbol{N_a}|}{L_c} \sum_{j:n_j \in \boldsymbol{N_a}} \left[\left(\frac{L_{cj}}{L_{xj}} - 1\right) \cdot w_a\right] \tag{14}$$

Equations 12 through 14 correspond to the tortuosity index formulation proposed by Baumgartner et al. (2019). In these equations, f_{SF} is a survey-frequency scaling factor introduced to properly account for the influence of survey distance in the magnitude of the tortuosity index. $\boldsymbol{N_i}$ and $\boldsymbol{N_a}$ represent the set of curve turns, where the j-th curve turn is represented as n_j, L_c is the borehole MD, L_{cj} is the j-th curve length, L_{xj} is the j-th curve chord (straight-line) length, and w_i and w_a are the weighting factors for inclination and azimuth, respectively. Readers can consult Baumgartner et al. (2019) for additional details on this tortuosity index estimation.

It is important to note from Equation 11 that, intuitively, this variable is expected to increase when the contact points (with the highest flexural rigidity in the BHA) traverse intervals where the tortuosity index increases rapidly.

3.2.6 Proximity of Contact Points to Zones with Potential Accumulation of Cuttings

This variable indicates whether the BHA is near an interval with potential cuttings accumulation. The cuttings accumulation along the borehole at time t, denoted as $\zeta(z,t)$, is determined using the transient cuttings transport model introduced by Fallah et al. (2020). The proximity of contact points to these intervals is then determined as follows:

$$c_t = \frac{1}{|\boldsymbol{\Pi}|} \sum_{\pi_i \in \boldsymbol{\Pi}} \sum_{b_j \in \boldsymbol{B}} \left| z_{\pi_i} - z_{b_j} \right| \tag{15}$$

Here, c_t is the mean proximity of contact points to intervals of cuttings accumulation, $\boldsymbol{\Pi}$ is the set of BHA contact points, π_i is the i-th contact point of a BHA, $\boldsymbol{B}$ is the set of all intervals with potential cuttings accumulation, b_j is the j-th interval with cuttings accumulation, z_{π_i} is the middle-point depth of the i-th contact point, z_{b_j} is the middle-point depth of the j-th interval with cuttings accumulation.

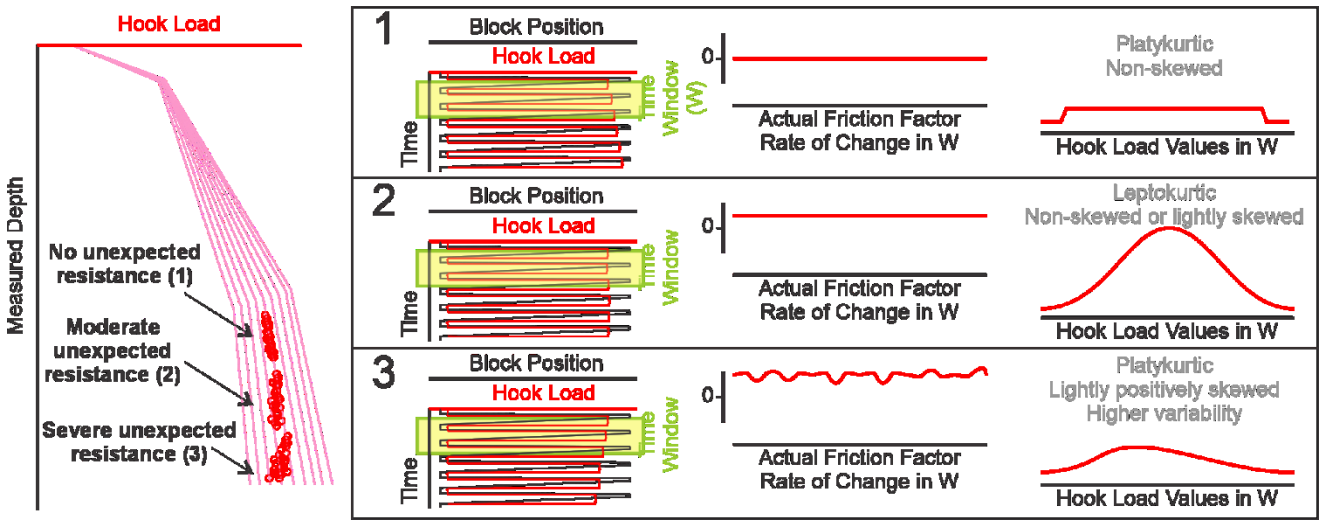

Figure 3: Behavior of some hook-load-related variables under different scenarios of resistance to pipe movement.

Figure 3 further illustrates the rationale behind some of the selected variables. In the absence of restrictions to pipe movement, the hook load signal, processed using windowing techniques, tends to be platykurtic with little or no skewness. This occurs because the hook load increases as more pipe stands are added to the string at the surface. When the string experiences some restriction due to increased friction, this friction counteracts the weight of the additional pipes, causing the hook load to remain almost unchanged while tripping in the hole. As a result, the hook load signal becomes leptokurtic (see example in Figure 4). Finally, under conditions of severe restriction (such as with BHA No. 8 in Well B), the hook load may actually decrease while tripping in, becoming platykurtic and possibly exhibiting some skewness toward lower hook loads.

It is important to note that a decrease in hook load while tripping in is sometimes expected, particularly in highly deviated wells. However, in these cases, the change in the back-calculated friction factor remains close to zero, as hook load observations fall within the expected line for hook load associated with a unique friction factor.

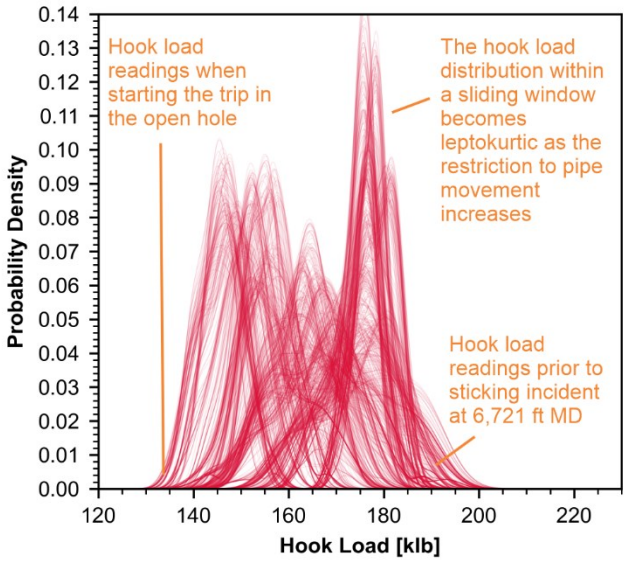

Figure 4: Hook load distribution within a sliding time window for the trip in the hole with BHA No. 14 in the well Utah FORGE 78B-32—which became stuck near the bottom.

3.3 Multi-Agent System Construction and Testing

Based on the selected variables, a fuzzy clustering model was constructed for each historical agent. The number of clusters was determined using the FPC criterion, as previously described. The criterion indicated that three clusters provided a better representation of the drilling conditions than two for the constructed historical agents. This additional cluster was associated with a 'moderate risk' of sticking, as it encapsulated conditions between those close to the sticking incident and those occurring much earlier.

Once all agents were constructed, we assembled the multi-agent system and tested it using data from well 16B(78)-32. Since the incident occurred while tripping, agents 16A(78)-32 and 58-32 remained idle, as they are only capable of assessing sticking risk while drilling. The real-time signals and contextual data from well 16B(78)-32 were processed by the active agents and transformed into their respective variable spaces. Within these spaces, the drilling conditions were evaluated using the pre-trained models to assess the associated sticking risk. This risk was determined by comparing the drilling conditions at each point in time to the centroid of the pre-identified risk-related clusters.

Finally, the sticking risk evaluations generated by all active agents [i.e., all agents except for 16B(78)-32, which was reserved for testing, and 16A(78)-32 and 58-32, which cannot predict while tripping] were aggregated by the risk aggregation agent, with their contributions weighted by the similarity of wells, as described in Section 2.3. Figure 5 shows the normalized sticking risk predicted by the risk aggregation agent, from the moment the drilling crew started tripping out of hole with BHA No. 3 to the moment the sticking incident occurred. The plot demonstrates the effectiveness of the proposed system to quantify the risk of sticking. It shows how the sticking risk progressively increased as the drillstring approached the sticking point, within a 35 min period, peaking just before the stuck pipe incident. Additionally, Figure 6 illustrates the contributions of the active agents in the final risk estimate, along with the interpreted sticking mechanism resulting from these contributions. Note that these contributions are scaled from 0 to 1 by the aggregation agent (see Equation 1).

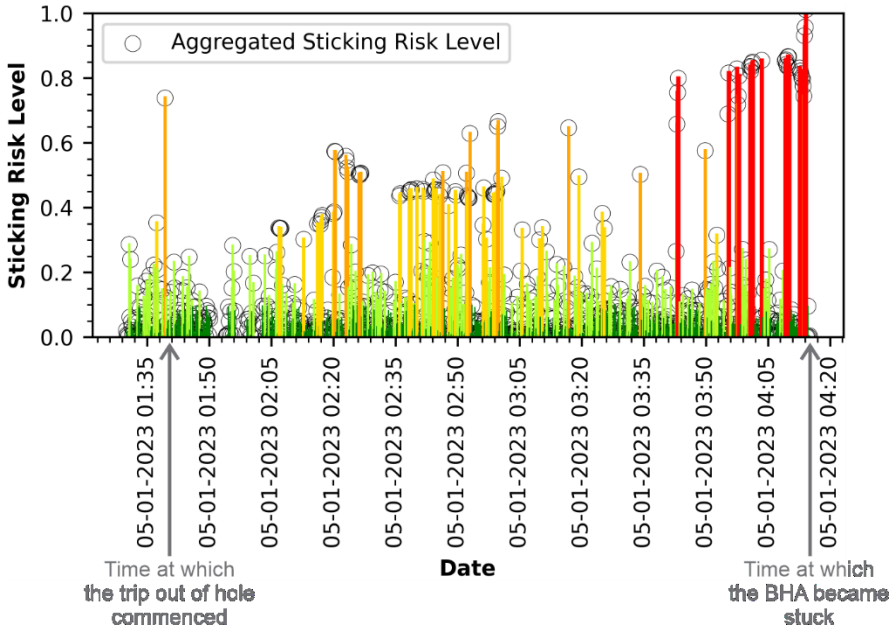

Figure 5: Sticking risk predicted with the proposed multi-agent system while tripping out of hole with BHA No. 3 in well Utah FORGE 16B(78)-32. The color indicates the risk level, which is also shown quantitatively on the vertical axis: green represents a low risk of sticking, yellow indicates a medium risk, and red signifies a high risk.

4. DISCUSSION

Results show that the sticking event in well 16B(78)-32 could have been effectively anticipated using the proposed multi-agent system—primarily by leveraging data from previous Utah FORGE wells. If this information had been available to the drilling crew during tripping out with BHA No. 3, they would have been forewarned of the potential sticking incident at 2,241 ft MD and the associated mechanisms. Preventative measures that could have been implemented to avoid the incident include: (1) connecting the top drive to pump out of hole instead of tripping on elevators, (2) stopping for a short circulation cycle, and (3) pumping a viscous sweep to evacuate potential cuttings dragged by the BHA while tripping on elevators.

Importantly, the multi-agent system can be implemented as a real-time tool, which is essential for preventing sticking incidents during well construction (Montes et al. 2024b). Additionally, this tool can address challenges associated with real-time prediction, such as handling missing or uncertain data, rig state (process) characterization, and data aggregation from different sources, particularly the integration of real-time and contextual data for variable derivation. While these challenges may lessen with the emergence of novel sensors and data-acquisition systems, they currently represent one of the primary obstacles to data-driven modeling for geothermal drilling optimization (Behounek and Ashok 2017, Rallo et al. 2022, Schultz et al. 2023).

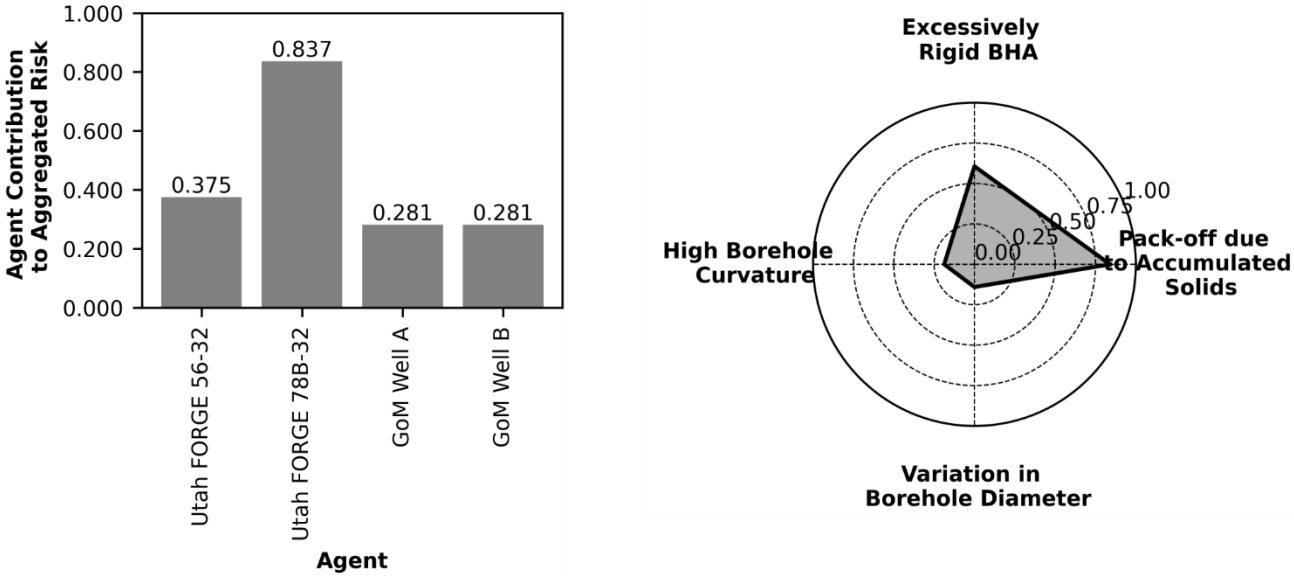

Figure 6: (left) Contribution of historical agents to the aggregated risk of sticking predicted in the Utah FORGE well 16B(78)-32. (right) Interpreted potential causes of sticking associated with the agents' contributions to the aggregated risk.

The variables used to build the historical agents proved effective for forewarning geometric- and annular pack-off-related sticking incidents, similar to those observed in the Utah FORGE wells. These variables account not only for statistical characteristics of real-time signals but also incorporate knowledge of the drilling context and insights from physics-based models. This combination is essential for differentiating between normal, expected conditions and risky, sticking-prone conditions, as illustrated in Figure 3. Such differentiation is crucial for avoiding spurious predictions and false warnings of sticking. For example, the hook load distribution within a sliding time window may become platykurtic and slightly skewed under both normal conditions and severe restriction to pipe movement. However, by incorporating knowledge about well trajectory and the back-calculated friction factor, we can determine whether this behavior is expected or indicative of a risky, abnormal condition.

Beyond the cases presented in this paper, other sticking mechanisms exist. As part of our future work, we plan to extend the proposed system in three key ways. First, we will expand the pool of variables used to estimate sticking risk. This will involve adding a second set of 'generic' agents that evaluate drilling conditions based on universally applicable criteria, such as the potential for induced borehole instability and the dependence of resistance to pipe movement on static pipe time—a clear indication of differential sticking (Dupriest et al. 2011). Second, we will add historical agents to broaden the coverage of sticking mechanisms, thereby increasing the 'database' of sticking signatures that will be searched in real time over streaming drilling data. Finally, we are in the process of compiling this multi-agent system into a flexible, web-based, service-oriented application that can integrate with various companies' data management systems for real-time stuck pipe prediction.

Lastly, the proposed solution can be extended to other types of drilling incidents, including lost circulation and premature or excessive bit wear. This extension would require engineering variable spaces capable of differentiating early signs of these incidents from normal conditions. For instance Rallo et al. (2022) proposed a variable space using Kohonen maps and k-means clustering to create a 2D space where drilling processes can be tracked and early signs of problems can be identified. Extending the multi-agent system to recognize signatures of other incidents could potentially reduce the number of false positives even further, allowing it to better differentiate symptoms of various incidents that may present as similar anomalies in surface signals, such as motor stalling and annular pack-off, where standpipe pressure may rapidly increase above the expected circulation pressure.

5. CONCLUSIONS

In this paper, we proposed a multi-agent solution for stuck pipe prediction. This solution not only predicts the risk of sticking but also provides insights into the potential mechanisms generating such risks, which is crucial for implementing appropriate preventative measures. It is also applicable in real time, allowing for timely actions to avoid costly incidents.

The solution was tested on the Utah FORGE well 16B(78)-32. The results presented in this paper lead to the following conclusions:

- The geothermal industry can benefit significantly from leveraging data collected during drilling operations. Drilling incident predictors consuming that data, such as the multi-agent system presented in this paper, can help avoid costly incidents in future drilling operations by effectively forewarning the drilling crew about existing risks. This enables the design and implementation of appropriate risk reduction plans. Such forewarning has the potential not only to lower the levelized cost of energy, which is highly sensitive to drilling costs, but also to facilitate the development of autonomous drilling solutions for the geothermal industry.

- The multi-agent system for stuck pipe prediction outlined in this paper demonstrates the value of drilling data, regardless of the well's purpose, across the entire drilling industry. While two of the agents in our system are related to deep offshore wells constructed for oil-and-gas extraction, their data can also be used to predict sticking incidents in geothermal well construction. This is because physics principles have universal applicability, e.g., mechanical sticking in an oil/gas well or geothermal well will have very similar signatures. Similarly, data collected during the drilling of the Utah FORGE wells can be utilized to forewarn incidents in oil and gas extraction wells.
- The selected variables successfully formed a variable space in which sticking and non-sticking conditions can be differentiated using a clustering model. The fuzziness introduced by this model provides valuable insights into the evolution of the sticking condition, from an incipient state, where minor or no restrictions are experienced, to a fully stuck condition, where the BHA cannot be moved downhole.
- The proposed multi-agent system for stuck pipe prediction can be employed for real-time risk assessment, providing the drilling crew with early indications of potential sticking. This information can then be used to effectively prevent these incidents from occurring.

While the focus of the particular solution described in this paper is on stuck pipe prediction, the framework is very versatile and can be applied to construct predictors for other costly, time-consuming drilling incidents, such as lost circulation events, wellbore breathing occurrences, well control incidents, etc.

6. ACRONYMS

A_i: i-th Historical Agent
BHA: Bottomhole Assembly
FPC: Fuzzy Partition Coefficient
GoM: Gulf of Mexico
GT: Geothermal
EGS: Enhanced Geothermal System
HWDP: Heavy Weight Drill Pipe
LCOE: Levelized Cost of Energy
LWD: Logging While Drilling
MD: Measured Depth
NPT: Non-Productive Time
OD: Outer Diameter (External Diameter)
PDC: Polycrystalline Diamont Compact
RSS: Rotary Steerable System
SBM: Synthetic-Based Mud
TD: Total Depth
WBM: Water-Based Mud

REFERENCES

Ahmed, A., Elkatatny, S., Abdulraheem, A., and Abughaban, M. 2020. Prediction of Lost Circulation Zones using Support Vector Machine and Radial Basis Function. Paper presented at the International Petroleum Technology Conference, Dhahran, Kingdom of Saudi Arabia, 13–15 January. IPTC-19628-MS. https://doi.org/10.2523/iptc-19628-ms.

AlMuhaideb, A. and Noynaert, S. 2021. A 20 Years Systemic Study of Drilling Practices in a Geothermal Venture Reveals Insightful Findings. Paper presented at the SPE Annual Technical Conference and Exhibition, Dubai, UAE, 21–23 September. SPE-206092-MS. https://doi.org/10.2118/206092-ms.

Baumgartner, T., Lin, C., Liu, Y., Mendonsa, A., and Zimpfer, D. 2019. Using Big Data to Study the Impact of Wellbore Tortuosity on Drilling, Completions, and Production Performance. Paper presented at the SPE/IADC International Drilling Conference and Exhibition, The Hague, The Netherlands, 5–7 March. SPE-194182-MS. https://doi.org/10.2118/194182-ms.

Beckers, K. F., Lukawski, M. Z., Anderson, B. J., Moore, M., and Tester, J. W. 2014. Levelized Costs of Electricity and Direct-Use Heat from Enhanced Geothermal Systems. *Journal of Renewable Sustainable Energy* **6**: 013141. https://doi.org/10.1063/1.4865575.

Behounek, M. and Ashok, P. 2017. Technology Update: Data Aggregation and Distribution With Human Factors Incorporated. *Journal of Petroleum Technology* **69** (09): 20–22. https://doi.org/10.2118/0917-0020-jpt.

Bezdek, J. C., Ehrlich, R., and Full, W. 1984. FCM: The Fuzzy C-Means Clustering Algorithm. *Computers & Geosciences* **10** (2): 191–203. https://doi.org/10.1016/0098-3004(84)90020-7.

Bowes, C. and Procter, R. 1997. *Drillers Stuck Pipe Handbook*, first edition. Ballater, Scotland, UK: Procter & Collins.

Brommer, M. and O'Sullivan, J. 2020. The Current Status of Deep Geothermal Energy. *First Break* **38** (10): 51–54. https://doi.org/10.3997/1365-2397.fb2020073.

Dupriest, F. E., Elks, W. C., and Ottesen, S. 2011. Design Methodology and Operational Practices Eliminate Differential Sticking. *SPE Drilling & Completion* **26** (01): 115–123. SPE-128129-PA. https://doi.org/10.2118/128129-pa.

Elahifar, B. and Hosseini, E. 2022. Machine Learning Algorithm for Prediction of Stuck Pipe Incidents Using Statistical Data: Case Study in Middle East Oil Fields. *Journal of Petroleum Exploration and Production Technology* **12** (7): 2019–2045. https://doi.org/10.1007/s13202-021-01436-3.

Fallah, A., Gu, Q., Saini, G., Chen, D., Ashok, P., van Oort, E., and Karimi Vajargah, A. 2020. Hole Cleaning Case Studies Analyzed with a Transient Cuttings Transport Model. Paper presented at the SPE Annual Technical Conference and Exhibition, Virtual, 26 - 29 October. SPE-201461-MS. https://doi.org/10.2118/201461-ms.

Feng, Y., Yang, H., Li, X., Zhang, S., Hu, H., and Wang, J. 2024. Interpretable Lost Circulation Analysis: Labeled, Identified, and Analyzed Lost Circulation in Drilling Operations. *SPE Journal* **29** (04): 1692–1709. SPE-218380-PA. https://doi.org/10.2118/218380-pa.

Hou, X., Yang, J., Yin, Q., Liu, H., Chen, H., Zheng, J., Wang, J., Cao, B., Zhao, X., Hao, M., and Liu, X. 2020. Lost Circulation Prediction in South China Sea using Machine Learning and Big Data Technology. Paper presented at the Offshore Technology Conference, Houston, Texas, USA, 4–7 May. OTC-30653-MS. https://doi.org/10.4043/30653-ms.

Inoue, T., Kaneko, T., Nakagawa, Y., Wada, R., Abe, S., and Yasutake, G. 2024. A Novel Approach of Data Science Incorporating Physical Knowledge for Early Stuck Pipe Detection. Paper presented at the ASME 2024 43rd International Conference on Ocean, Offshore and Arctic Engineering, Singapore, Singapore, 9–14 June. OMAE2024-125728. https://doi.org/10.1115/omae2024-125728.

Johancsik, C. A., Friesen, D. B., and Dawson, R. 1984. Torque and Drag in Directional Wells-Prediction and Measurement. *Journal of Petroleum Technology* **36** (06): 987–992. SPE-11380-PA. https://doi.org/10.2118/11380-pa.

Kaneko, T., Inoue, T., Nakagawa, Y., Wada, R., Abe, S., Yasutake, G., and Fujita, K. 2024. Hybrid Approach Using Physical Insights and Data Science for Stuck-Pipe Prediction. *SPE Journal* **29** (02): 641-650. SPE-218013-PA. https://doi.org/10.2118/218013-pa.

Liu, M., Song, X., Zhu, Z., Li, G., Xiao, H., Fu, L., Pan, T., Li, X., and Yang, Y. 2024. Inertial Effect of Drill Pipe Friction Trend and Early Warning of Stuck Pipe. Paper presented at the SPE Annual Technical Conference and Exhibition, New Orleans, Louisiana, USA, 23–25 September. SPE-220991-MS. https://doi.org/10.2118/220991-ms.

Magana-Mora, A., AlJubran, M., Ramasamy, J., AlBassam, M., Gooneratne, C., Gonzalez, M., Thiel, T., and Deffenbaugh, M. 2021. Machine-Learning for the Prediction of Lost Circulation Events - Time Series Analysis and Model Evaluation. Paper presented at the SPE Middle East Oil & Gas Show and Conference, event canceled, 28 November–1 December. SPE-204706-MS. https://doi.org/10.2118/204706-ms.

Marck, J. and Detournay, E. 2016. Influence of Rotary-Steerable-System Design on Borehole Spiraling. *SPE Journal* **21** (01): 293–302. SPE-174554-PA. https://doi.org/10.2118/174554-pa.

Mitchell, J. 2014. *Trouble-Free Drilling: Stuck Pipe Prevention*, third edition. The Woodlands, Texas, USA: Drilbert Engineering.

Montes, A. C., Ashok, P., and van Oort, E. 2023. Stuck Pipe Prediction in Utah FORGE Geothermal Wells. Paper presented at the SPE Annual Technical Conference and Exhibition, San Antonio, Texas, USA, 16–18 October. SPE-214783-MS. https://doi.org/10.2118/214783-ms.

Montes, A. C., Ashok, P., and van Oort, E. 2024a. Comparing Drilling Anomaly Prediction by Purely Data-Driven and Hybrid Analysis Methods - Case Study of Utah FORGE Geothermal Wells. Paper presented at the IADC/SPE International Drilling Conference and Exhibition, Galveston, Texas, USA, 5–7 March. SPE-217737-MS. https://doi.org/10.2118/217737-ms.

Montes, A. C., Ashok, P., and van Oort, E. 2024b. Review of Stuck Pipe Prediction Methods and Future Directions. Paper presented at the SPE Annual Technical Conference and Exhibition, New Orleans, Louisiana, USA, 23–25 September. SPE-220725-MS. https://doi.org/10.2118/220725-ms.

Montes, A. C., Sudyodprasert, K., Wu, Y., Ashok, P., and van Oort, E. *In press*. Automated Drilling and Production Event Detection Using Advanced Time-Series Pattern Recognition Techniques. Paper to be presented at the SPE/IADC International Drilling Conference and Exhibition, Stavanger, Norway, 4–7 March 2025. SPE-223795-MS.

Othman, E. B., Gomes, D., Tengku Bidin, T. E. B., Meor Hashim, M. M. H., Yusoff, M. H., Arriffin, M. F., and Ghazali, R. 2022. Application of Machine Learning to Augment Wellbore Geometry-Related Stuck Pipe Risk Identification in Real Time. Paper presented at the Offshore Technology Conference Asia, Kuala Lumpur, Malaysia, 22–25 March. OTC-31695-MS. https://doi.org/10.4043/31695-ms.

Pang, H., Meng, H., Wang, H., Fan, Y., Nie, Z., and Jin, Y. 2022. Lost Circulation Prediction Based on Machine Learning. *Journal of Petroleum Science and Engineering* **208**: 109364. https://doi.org/10.1016/j.petrol.2021.109364.

Pastusek, P. and Brackin, V. 2003. A Model for Borehole Oscillations. Paper presented at the SPE Annual Technical Conference and Exhibition, Denver, Colorado, USA, 5–8 October. SPE-84448-MS. https://doi.org/10.2118/84448-ms.

Purba, D., Adityatama, D., Agustino, V., Fininda, F., Alamsyah, D., and Muhammad, F. 2020. Geothermal Drilling Cost Optimization in Indonesia: A Discussion of Various Factors. Paper presented at the 45th Workshop on Geothermal Reservoir Engineering, Stanford, California, USA, 10–12 February. SGP-TR-216.

Rallo, R., Carbonari, R., Ton, D., Ashari, R., Ashok, P., Bonnevile, A., Bour, D., Cladouhos, T., Garrison, G., Horne, R., van Oort, E., Petty, S., Schultz, A., Sørlie, C., Thorbjornsson, I., Uddenberg, M., and Weydt, L. 2022. A Probabilistic Approach to Model and Optimize Geothermal Drilling. Paper presented at the 47th Workshop on Geothermal Reservoir Engineering, Stanford, California, USA, 7–9 February. SGP-TR-223.

Rotimi, O. J., Ukwu, D. N., Zhenli, W., Liang, Y., Ameloko, A. A., Ogunkunle, T. F., Oyeyemi, K. D., Kouamelan, K. S., Asaboro, U. F., and Onuigbo, I. S. 2021. Sequential Prediction of Drilling Fluid Loss Using Support Vector Machine and Decision Tree Methods. Paper presented at the SPE Nigeria Annual International Conference and Exhibition, Lagos, Nigeria, 2–4 August. SPE-207185-MS. https://doi.org/10.2118/207185-ms.

Salehi, Y., Ziada, A., and Rawahi, Z. 2022. Significant Stuck Pipe Event Reduction Realized Through Structured Holistic Approach Machine Learning and Artificial Intelligence. Paper presented at the ADIPEC, Abu Dhabi, UAE, 31 October–3 November. SPE-211738-MS. https://doi.org/10.2118/211738-ms.

Sanyal, S., Morrow, J., Butler, S., and Robertson-Tait, A. 2007. Cost of Electricity from Enhanced Geothermal Systems. Paper presented at the 32nd Workshop on Geothermal Reservoir Engineering, Stanford, California, USA, 22–24 January. SGP-TR-183.

Schultz, A., Ashok, P., Bonnevile, A., Bour, D., Carbonari, R., Cladouhos, T., Garrison, G., Horne, R., Kaldal , G., Petty, S., Rallo, R., Sørlie, C., Ton, D., Uddenberg, M., van Oort, E., and Weydt, L. 2023. Drilling the Perfect Geothermal Well: An International Research Coordination Network for Geothermal Drilling Optimization Supported by Deep ML and Cloud Based Data Aggregation. Paper presented at the 48th Workshop on Geothermal Reservoir Engineering, Stanford, California, USA, 6–8 February. SGP-TR-224.

Shahri, M. P., Oar, T. T., Safari, R., Karimi, M., and Mutlu, U. 2015. Advanced Semianalytical Geomechanical Model for Wellbore-Strengthening Applications. *SPE Journal* **20** (06): 1276–1286. SPE-167976-PA. https://doi.org/10.2118/167976-pa.

Thonhauser, G., Wallnoefer, G., Mathis, W., and Ettl, J. 2007. Use of Real-Time Rig-Sensor Data To Improve Daily Drilling Reporting, Benchmarking, and Planning—A Case Study. *SPE Drilling & Completion* **22** (03): 217–226. SPE-99880-PA. https://doi.org/10.2118/99880-pa.

van Oort, E., Chen, D., Ashok, P., and Fallah, A. 2021. Constructing Deep Closed-Loop Geothermal Wells for Globally Scalable Energy Production by Leveraging Oil and Gas ERD and HPHT Well Construction Expertise. Paper presented at the SPE/IADC International Drilling Conference and Exhibition, Virtual, 8–12 March. SPE-204097-MS. https://doi.org/10.2118/204097-ms.

Wang, H. T., Wen, X., Zhang, R., Song, X. Z., Zhu, Z. P., Yao, X. Z., and Han, L. 2023a. Intelligent Lost Circulation Early Warning Method Based on HALSTM Network. *Proc.,* 57th U.S. Rock Mechanics/Geomechanics Symposium, Atlanta, Georgia, USA, 25–28 June, https://doi.org/10.56952/arma-2023-0093.

Wang, J., Guan, Z., Liu, M., Song, X., and Wang, Z. 2023b. Drilling Stuck Probability Intelligent Prediction Based on LSTM Considering Local Interpretability. Paper presented at the 57th U.S. Rock Mechanics/Geomechanics Symposium, Atlanta, Georgia, USA, 25–28 June. ARMA-2023-0326. https://doi.org/10.56952/arma-2023-0326.

Winn, C., Dobson, P., Ulrich, C., Kneafsey, T., Lowry, T. S., Akerley, J., Delwiche, B., Samuel, A., and Bauer, S. 2023. Context and Mitigation of Lost Circulation During Geothermal Drilling in Diverse Geologic Settings. *Geothermics* **108**: 102630. https://doi.org/10.1016/j.geothermics.2022.102630.

Yost, K., Valentin, A., and Einstein, H. H. 2015. Estimating Cost and Time of Wellbore Drilling for Engineered Geothermal Systems (EGS) – Considering Uncertainties. *Geothermics* **53**: 85–99. https://doi.org/10.1016/j.geothermics.2014.04.005.

APPENDIX A: STUCK PIPE INCIDENTS IN WELLS A AND B

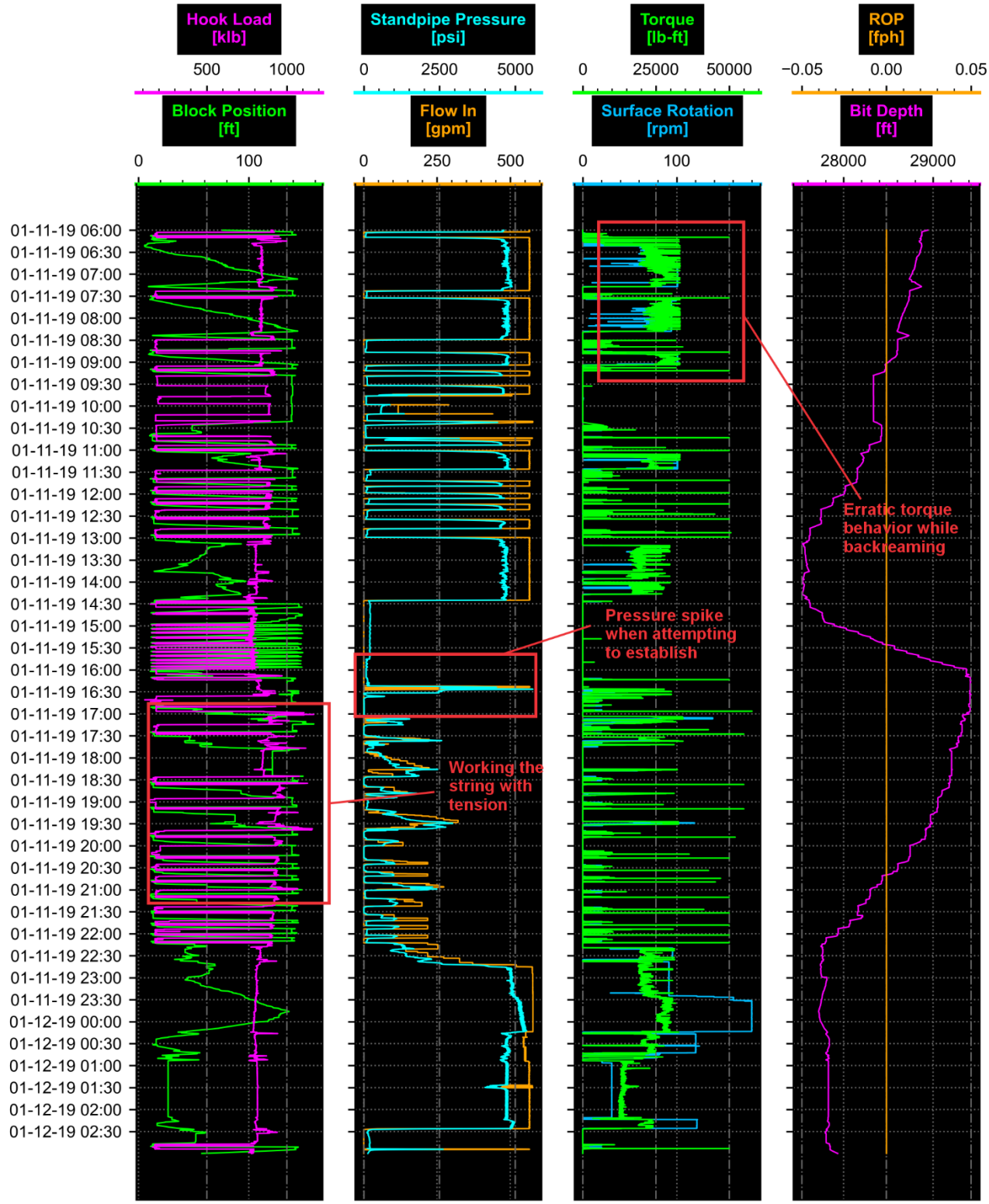

Figure A1: Real-time signals collected in Well A during the trip out of hole in the 9-7/8 in. borehole section with BHA No. 5.

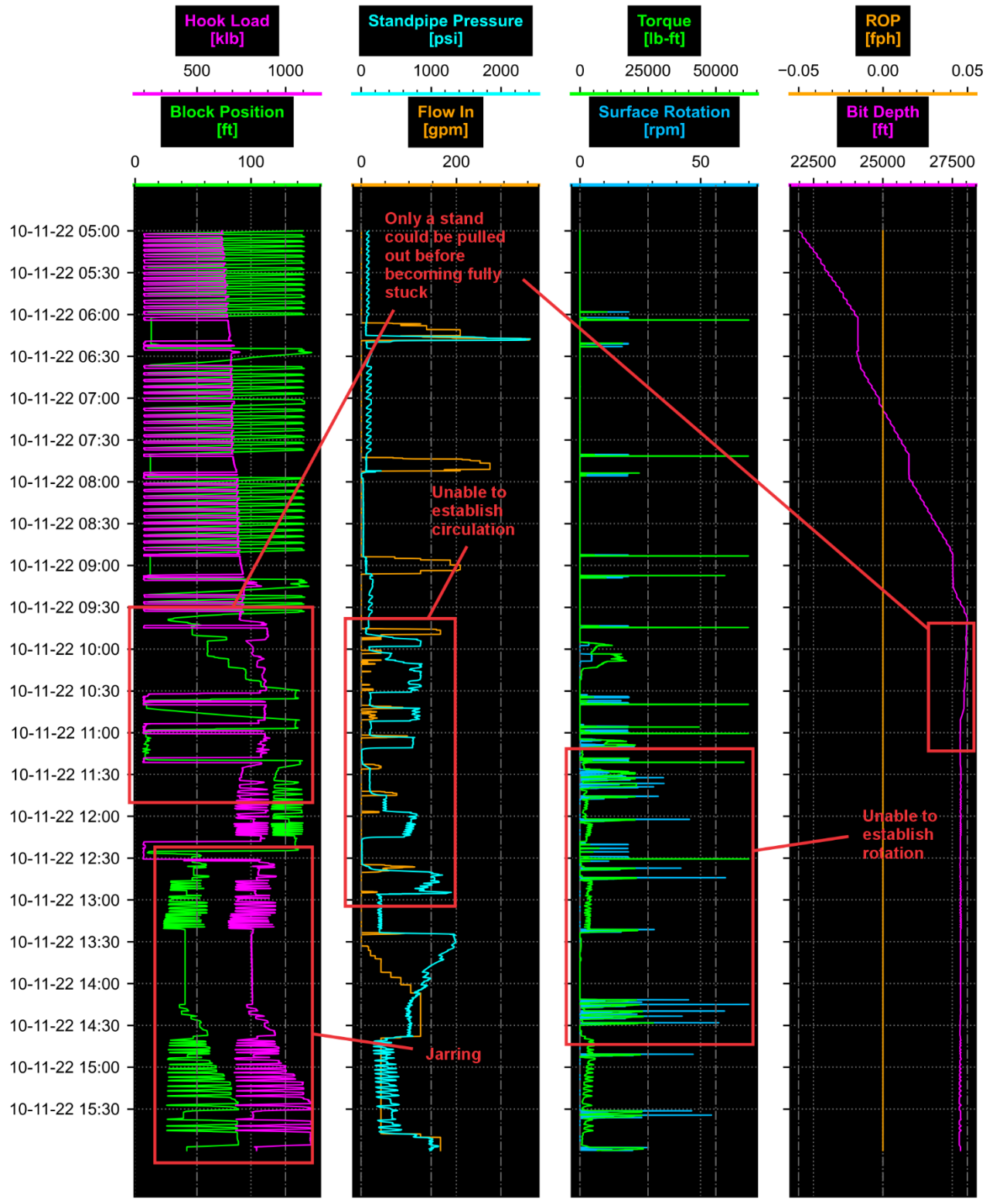

Figure A2: Real-time signals collected in Well B during the trip in the hole in the 5-7/8 in. borehole section with BHA No. 6 (the displacement BHA).

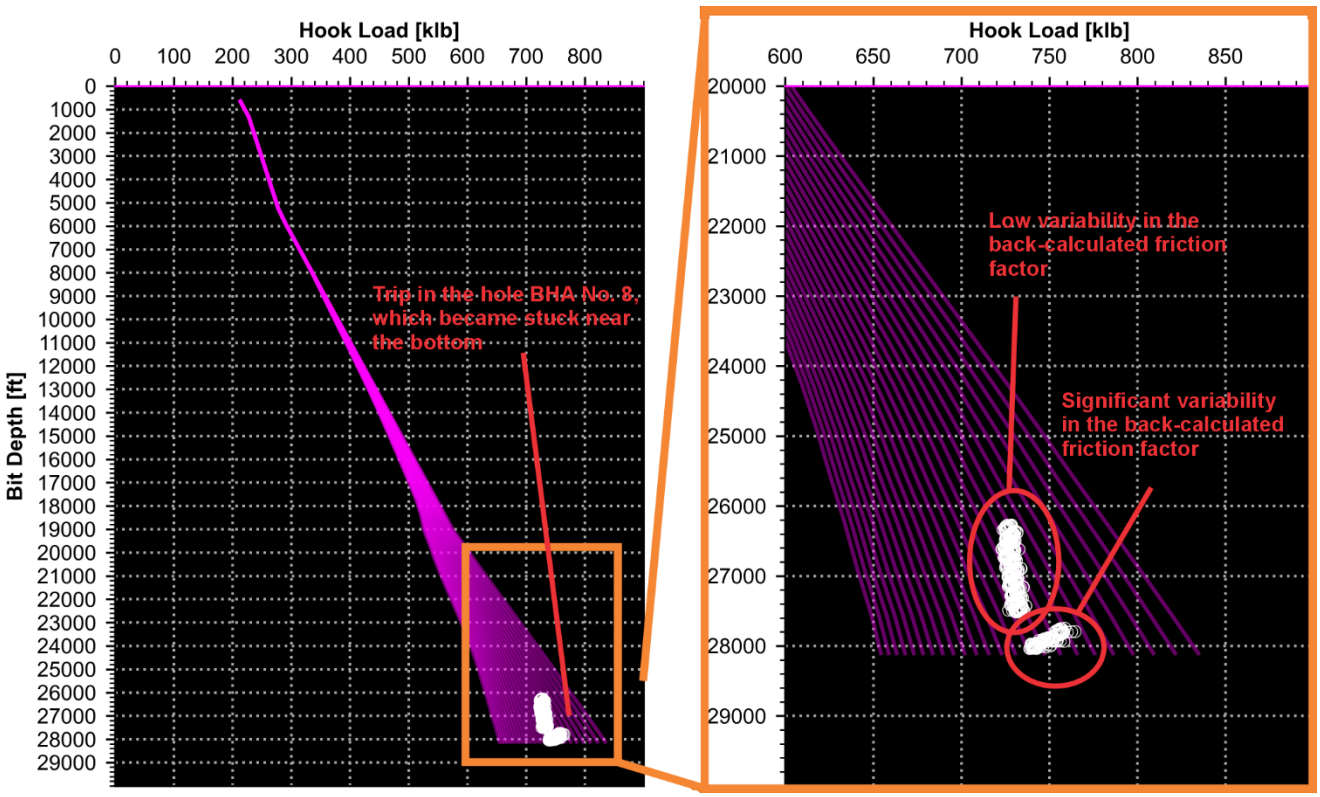

Figure A3: Torque-and-drag simulation of the trip in the 5-7/8 in. borehole section with BHA No. 8 in Well B.